Searching for pulsars with LOFAR

Coenen, T.

Publication date
2013

CHAPTER 3

THE LOFAR PILOT PULSAR SURVEY

Thijs Coenen & LOFAR Pulsar Working Group
Published as Proc. of IAU Symposium 291 (2013), p. 229
To be submitted to Astronomy & Astrophysics (2013)

Abstract — Using the Low Frequency Array (LOFAR) radio telescope, we observed a large fraction of the northern sky ($\sim 1.4 \times 10^4$ sq. deg) to search for pulsars and fast radio transients, i.e. any sub-second, dispersed radio burst. Each observation consisted of 7 individual fields-of-view (FoVs) formed by incoherently summing the high-band stations in the LOFAR core (each split into two so-called sub-stations). This technique allowed for a very large FoV of ~ 75 sq. deg per pointing. Although these data were collected during LOFAR's commissioning stage, and consequently suffer from poor calibration and early hardware issues, we have been able to re-detect 54 known pulsars in periodicity searches, of which 18 were also detected in single-pulse searches of the data. A further 2 pulsars were re-detected only through their single pulses and 9 re-detected by folding on known rotational ephemerides. The large product of field-of-view and dwell time (57 min per pointing) allows us to derive a competitive limit on the rate of bright ($S_{150} > 107$ Jy), highly dispersed single bursts of $< 1.5 \times 10^2$ per day over the full sky at these low radio frequencies. This limit assumes that scattering does not significantly affect the detectability of the signal. This pilot survey demonstrates LOFAR's ability to perform efficient all-sky surveys for pulsars and fast transients and sets the stage for a repeated all-sky survey using LOFAR's full sensitivity. It also serves as the first prototype for a pulsar survey using the planned low-frequency aperture array of the Square Kilometer Array (SKA).

3.1 INTRODUCTION

THE discovery of pulsars was made at the low radio frequency of 81.5 MHz with the Cambridge Inter Planetary Scattering (IPS) array (Hewish et al., 1968). Since then, however, most pulsar surveys have avoided low radio frequencies (< 300 MHz) because of several interstellar propagation effects that become increasingly relevant towards low frequency and which complicate the detection of pulsar signals. First, since pulsar signals are dispersed by free electrons along the line-of-sight, the signal is smeared in time across a finite bandwidth, with lower frequencies arriving progressively later. Although this effect can be corrected for precisely, it scales as ν^{-2} and therefore requires smaller frequency channels at low frequencies to keep intra-channel smearing in check (Lorimer & Kramer, 2005). Thus, for a blind search over the possible range of dispersion measures (having a exponential tail with a scattering time-scale strongly dependent on observing frequency. This time-scale was measured to increase as $\nu^{-3.9}$ by Bhat et al. (2004), and is consequently a major limitation for low-frequency observations, especially since there is no practical way to correct for this effect in a blind pulsar survey. Lastly, the sky background temperature (T_{sky}) scales as $\nu^{-2.6}$ (Lawson et al., 1987) which impacts the detectability of radio pulsars, but can be mitigated somewhat by observing off of the Galactic plane (where T_{sky} is highest).

The aforementioned drawbacks to low-frequency pulsar observations are partially compensated for by the fact that pulsars are intrinsically brighter at low frequencies. In general they have steep power-law spectra: $\nu^{-1.8}$ (Maron et al., 2000), but some pulsars show even steeper spectra ($S \propto \nu^{-2}$ - ν^{-4}). Previous studies have determined that many pulsar spectra turn over toward lower frequencies, and peak in the LOFAR band (Malofeev et al., 2000). Whether all pulsars do this, and what is the average low-frequency spectral behavior is still somewhat of an open question however and is being investigated using the large fractional bandwidth that LOFAR provides[1]. The combination of this intrinsic brightness increase with the potential for wider radio beams, exposing pulsars that miss Earth at other frequencies, makes the low-frequency regime an interesting, and until now mostly unexplored, domain for pulsar searches. For a more detailed discussion of these effects, as well as other considerations, see Stappers et al. (2011).

It is expected that the unique spectral window of the LOFAR pulsar surveys will complement the known population of pulsars that have been found searching at 350 and 1400 MHz. For instance, we will learn more about the spectral distribution of the population and whether there are any very low-luminosity, nearby sources still to be

[1] LOFAR can instantaneously observe 80 MHz of bandwidth from either 10−90 MHz or 110−190 MHz.

found. Finding new pulsars in general serves a wide range of scientific goals, as outline in Chapter 1.

Despite the unavoidable complications of low-frequency pulsar observations and the success of surveys at higher radio frequencies — typically around 430 MHz (e.g. Hulse & Taylor, 1975; Manchester et al., 1996) or 1400 MHz (e.g. Manchester et al., 2001) — some low-frequency surveys have been performed. The Cambridge IPS array was again used in 1993 – 1994 to perform a second pulsar survey at 81.5 MHz, though that survey had limited time/frequency resolution (by today's standards) and did not discover any new pulsars (Shrauner et al., 1998). Re-analysis of the Gauribidanur pulsar survey data, taken between 2002 – 2006 at 34.5 MHz, resulted in the first (potential) radio detection of Fermi pulsar J1732−3131 (Maan et al., 2012) — a source that might only be detectable below 50 MHz. Several successful surveys have recently been conducted using the Green Bank Telescope (GBT) at frequencies around 350 MHz (arguably on the limit of what we call "low frequency" in this context) and a complete survey of the northern celestial hemisphere, the Green Bank Northern Celestial Cap (GBNCC) survey, is underway (Stovall et al., in prep.). With their high time and frequency resolution, these low-frequency GBT surveys have been successful at discovering over 100 normal and millisecond pulsars so far (Hessels et al., 2008; Boyles et al., 2013; Lynch et al., 2013). Using the Westerbork Synthesis Radio Telescope (WSRT), a survey of the Cygnus region was performed at 328 MHz and led to the discovery of 3 new pulsars (Janssen et al., 2009). Though the pulsar yield was low, this was a pioneering project in terms of demonstrating how to use a dish-based radio interferometer for pulsar searching. The Ukrainian UTR-2 telescope recently did a census of known pulsars in the northern sky (more precisely $-10° < \delta \leq 90°$) in the band 16.5 – 33.0 MHz, re-detecting 40 out of 74 nearby ($DM < 30\,pc\,cm^{-3}$) pulsars with periods longer than 0.1s from the ATNF pulsar database[2] (Zakharenko et al., 2013). Nonetheless, the low-frequency end of the radio window, and especially the 100 – 200 MHz range where many pulsar spectra are believed to peak (Malofeev et al., 2000), remains under-explored by blind pulsar surveys using high time and frequency resolution combined with high sensitivity and large instantaneous field-of-view.

With its high sensitivity at low frequencies (10 – 90 MHz and 110 – 240 MHz) and efficient surveying capabilities, the Low Frequency Array (LOFAR; van Haarlem et al., 2013) is set to open the lowest radio frequencies to efficient pulsar surveys. LOFAR was designed and constructed by ASTRON, and is operated by the International LOFAR Telescope (ILT) foundation. Its multibeaming capability allows LOFAR to cover a large part of the sky quickly and its huge collecting area, wide fractional bandwidth and capability to store and process hundreds of terabytes of high-resolution data

[2]See Manchester et al. (2005)

make it a powerful instrument. For a general overview of LOFAR's pulsar observing capabilities and some early commissioning results we refer the reader to Stappers et al. (2011); for more information about the strategies behind pulsar surveys with LOFAR see van Leeuwen & Stappers (2010).

LOFAR underwent commissioning from 2008 – 2012 and as part of this effort the LOFAR Pulsar Working Group (PWG) performed two pulsar surveys in order to debug the system, create the necessary processing pipelines, and to identify unexpected challenges. The first such survey, using data from 2010 December, is called the LOFAR Pilot Pulsar Survey (LPPS)[3]. All LPPS survey observations consist of 7 beams, each formed by incoherently adding the signals from between 17 and 44 available LOFAR high-band sub-stations. These 7 beams instantaneously cover a total of 75 sq. degrees of sky[4] with a bandwidth of 6.8 MHz each. The large FoV of an LPPS pointing allowed a large fraction of the sky to be observed in relatively little observing time even if long dwell times of 57 minutes were used. The initial plan was for LPPS to cover the entire northern hemisphere and part of the southern celestial hemisphere down to $-30°$ declination. However when it became possible for LOFAR to form sensitive beams by coherently adding the station signals we shifted efforts to this new mode (the so-called "tied-array mode"; Chapter 4) and the LPPS observing campaign ended. Even taking into account failed observations LPPS still covered 34% of the full sky.

The LPPS survey has relatively limited time resolution (0.655-ms samples) compared with other state-of-the-art pulsar surveys and thus is targeted at slowly rotating pulsars as well as single, bright, dispersed bursts with millisecond durations. At the time of the survey, the low time resolution was necessary in order to ease the post-processing load, though recording much higher time resolution (down to 5-μs samples) is now achievable with LOFAR. The long dwell times of the LPPS pointings means that the survey is highly sensitive to intermittent pulsars, rotating radio transients (RRATs) and other fast radio transients in general. In total, LPPS has provided the equivalent of 5.4 minutes of *all-sky* coverage. No previous all-sky survey for fast transients has had a comparably large product of field-of-view (FoV) and integration time at such high sensitivity, and thus in addition to being a sensitive pulsar survey LPPS is also exploring new parameter space for rare, bright, and fast radio transients.

In order to detect potentially bright extra-galactic bursts, as well as anomalous, highly dispersed Galactic events, we searched our data up to a DM of 3000 pc cm^{-3}. This is a much larger DM than predicted for any typical line-of-sight by the NE2001 model of

[3]The second commissioning survey, entitled LOFAR Tied-Array Survey (LOTAS), is presented in Chapter 4.

[4]Using the full width at half maximum of the beam to measure field-of-view; the beams were spaced at the first null of LOFAR's core stations.

the electron density in our Galaxy away from the Galactic center (Cordes & Lazio, 2002). Signals with such high DMs may also be highly scattered, though this depends on the position of the scattering screen relative to the observer and source. In other words, DM depends on the number of free electrons along the line-of-sight, while scattering depends on their distribution. Though there is an observed relation between DM and scattering delay in the Galaxy (Bhat et al., 2004), this relation has more than an order-of-magnitude scatter and any single line-of-sight may deviate significantly from the average relation. Furthermore, it is unlikely that the ionized inter-galactic medium is distributed in a similar way to the Galactic inter-stellar medium. In any case, because of heavy downsampling in time, this high-DM part of the search added only a few percent to the total processing time and was deemed a valuable exercise.
In this chapter we present the LPPS survey. In Section 3.2 we describe our observations, in Section 3.3 the analysis, and in Section 3.4 we present the results of LPPS. In Section 3.5 we discuss some of the implications, while in Section 3.6 we finish with conclusions and future work.

3.2 OBSERVATIONS

3.2.1 SURVEY OBSERVATIONS

PULSAR observations are taken in LOFAR's so-called *beam-formed* observational modes (Stappers et al., 2011). Unlike LOFAR's interferometric imaging mode, these modes provide sub-millisecond time resolution at the cost of spatial resolution on the sky, because the cross-correlations between antenna stations are not stored. Each combined array beam effectively acts as a single pixel on the sky, and LOFAR can achieve a very large FoV by forming several, up to hundreds, of beams simultaneously (Romein et al., 2010).
Efficient pulsar surveys require high sensitivity, a large FoV and the ability to quickly determine a pulsar's position (which is the basis for all further follow-up work). LOFAR provides both a large FoV (>10 deg^2) and the ability to constrain positions to a few arcminutes, in the case of beam-formed data, and *arcseconds* in the case of imaging data. Incoherent addition of the LOFAR station beams maintains the large FoV of the single stations — $\sim 5.5°$ full width at half maximum (FWHM) in the LOFAR high band for LOFAR core high-band sub-stations — while increasing the overall sensitivity as the square root of the number of stations being added. For LPPS this dependence on the number of stations is complicated slightly because high band antenna (HBA) stations of two different sizes are combined: 48-tile remote stations

and 24-tile core sub-stations. With the gain G for a certain LOFAR configuration we then get

$$G \propto \frac{n_{\text{core}} + 2n_{\text{remote}}}{\sqrt{n_{\text{core}} + n_{\text{remote}}}}, \tag{3.1}$$

where n_{remote} is the number of remote stations and n_{core} the number of core stations used for that observation. Upon the discovery of a pulsar, coherent addition, in which the station beams are added in phase, narrows LOFAR's FoV and increases the sensitivity directly with the number of stations that are combined, allowing the pulsar's position to be determined more precisely. These modes can be used simultaneously, and standard correlation products can also be produced.

The LPPS survey was designed to take advantage of a relative lull in commissioning observations around the holiday period of December 2010 — in order to do a quick survey of the northern sky and to build and test the LOFAR pulsar search pipeline (whose construction was a significant part of the work behind this thesis). LPPS used the LOFAR system as it existed around the end of 2010, i.e. several tens of *not yet calibrated* Dutch LOFAR stations and the, then still newly commissioned, capability to form multiple beams at the station level.

The fact that LOFAR was not yet fully calibrated and properly monitored for hardware failures caused some major issues with data quality, as did the still rudimentary interference excision practices that were then in place. In Section 3.3.4 we describe the steps we took to mitigate these issues, which largely took the form of ignoring data sets that were obviously affected by system hardware or data-recording problems and radio frequency interference (RFI).

The survey was carried out using the LOFAR HBA stations. As the survey progressed, more stations became available. Initial observations used 13 core stations of 24 HBA tiles each plus 4 remote stations of 48 tiles each (for a complete description of the station configurations, see van Haarlem et al., 2013). Toward the end of the survey, this number had increased to 38 core and 6 remote stations. These were used to form 7 sets of incoherently summed station beams (also known as sub-array pointings), i.e. at the LOFAR station level 7 beams were formed and at the LOFAR Blue Gene P correlator/beam-former these beams were incoherently summed. The bandwidth of beams created at the station level is constrained by the available network bandwidth to the Central Processing (CEP) system (about 3 Gb/s for each station); this network bandwidth corresponds to about 48 MHz of observing bandwidth (using 16-bit samples), which can be spread anywhere in the LOFAR observing band (see van Haarlem et al., 2013, for a more detailed description of this capability). With 7 station beams, each is restricted to 1/7th of the total available bandwidth. For LPPS that means each beam has 6.8 MHz bandwidth, which was chosen to lie in the range

from 138.96 – 145.79 MHz, not too far from the peak sensitivity of the HBA elements. This band was subdivided into 560 channels of 12.21 kHz each recorded at a time resolution of 0.655 ms.
Given the central observing wavelength λ of 2.1 m ($\nu = 142$ MHz) and station sizes D of 30.8 m (core) and 41.1 m (remote; Stappers et al., 2011), the incoherent beams are quite broad. The theoretical circular-aperture FWHM (Kraus et al., 1986, Eq. A27.1) is $1.01\lambda/D$=4.1°(core) / 3.0°(remote). The 7 beams of each survey pointing were arranged in a honeycomb fashion with the beams touching at the core stations' first null, with beam centers separated by $1.22\lambda/D$=4.7°. As the HBA stations are not actually perfectly circular, and as two types of stations were added, the resulting FoV that was achieved can potentially differ from the theoretical numbers quoted above. We have thus performed full-wave EM simulations on HBA stations, and have modeled the incoherent summation of the sets of stations used (Wijnholds et al., 2012). The results for a representative set of stations are shown in Figures 3.1 and 3.2; Figure 3.1 shows that the LPPS beam pointed at the zenith is well-behaved and circular, with a FWHM of 3.7°. The farther-out side lobes of this beam pattern still provide sensitivity at the -30 dB level, as shown in Figure 3.2. While tracking the central pointing, a very strong off-center source may thus be detected drifting in and out of the 7 stations beams, as shown in Figure 3.14.

3.3 ANALYSIS

3.3.1 PIPELINE PROCESSING

THE LPPS data reduction was performed on the CEP cluster in Groningen, the Netherlands, and the Hydra cluster at the University of Manchester. The raw beam-formed data from LOFAR in 2010 December was not in a format that can be read directly by standard pulsar search software. Therefore a work-around had to be devised; for LPPS data processing the raw beam-formed LOFAR data were converted to PRESTO[5] (Ransom, 2001) sub-band files. These sub-band files are normally an intermediate data product created during sub-band dedispersion, but were sufficient to work with the LPPS data. For LPPS, each of these sub-band files corresponds to one of the 560 frequency channels. Further search processing was handled by a parallelized Python pipeline based on routines in the PRESTO pulsar search package (Ransom, 2001), and written as part of this thesis. This pipeline automates the process

[5] https://github.com/scottransom/presto

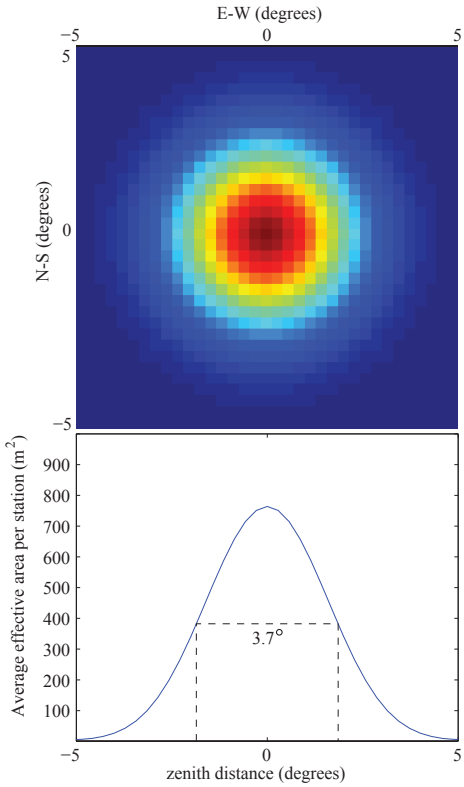

Figure 3.1: The simulated incoherently summed array beam for 13 core plus 4 remote stations (Wijnholds et al., 2012). The response of the stations was simulated for the LPPS 139-146 MHz band. Individual simulated HBA stations were rotated with respect to the North for an even distribution within the simulated set — as was done with the actual stations in the field. Top panel: the overall beam shape as seen to the zenith. Bottom panel: An E-W cut through the beam shape, expressed in units of effective collecting area on a linear scale. These same linear units apply to the color scale in the top plot. The FWHM of this station beam is 3.7°.

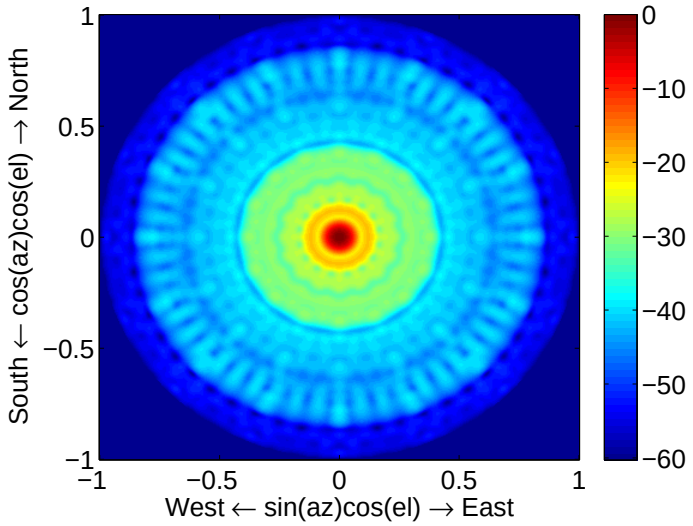

Figure 3.2: The incoherently summed array beam projected on the whole sky, using the same set of stations as Figure 3.1. Here the sensitivity is plotted on a logarithmic scale, such that the sidelobes between -25 and -30 dB are visible (Wijnholds et al., 2012).

of RFI excision, dedispersion, acceleration and single-pulse searching, and, lastly, sifting and folding of the best candidates. First, a frequency-time mask is created for each data set using PRESTO's `rfifind` utility. Frequencies known to generally contain significant amounts of RFI are also masked; this list was compiled by making a histogram of RFI occupancy versus frequency for all LPPS data sets. The data is then dedispersed to 3487 trial-DMs out to a maximum DM of 3003.6 pc cm^{-3}. As previously mentioned, this high maximum value of DM was chosen in the hopes of finding short, highly dispersed extragalactic bursts such as those reported by Lorimer et al. (2007) and Thornton et al. (2013). At the lowest DMs no downsampling is performed and the trial-DM spacing is 0.05 pc cm^{-3}, whilst at the very highest DMs the data is downsampled 64 times and the trial-DMs are spaced in steps of 5 pc cm^{-3}. The dedispersion is performed by PRESTO's `mpiprepsubband`, whilst applying the aforementioned mask and performing zero-DM filtering (Eatough et al., 2009). The latter technique removes (broad-band) interference at $DM = 0$ pc cm^{-3} from the data as that is generally where man-made radio emission occurs. Zero-DM filtering does not mitigate intrinsically frequency swept RFI like the radio emission of the HAMSAT

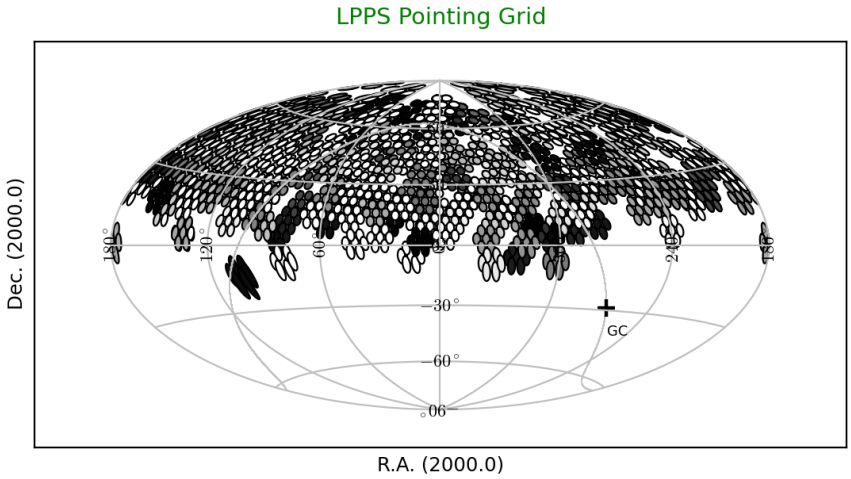

Figure 3.3: The total sky coverage achieved by LPPS, illustrating the extremely large overall survey footprint, spanning 34% of the celestial sphere. When projected on the sky, LPPS beams that are pointed away from zenith become elongated (for reference, the latitude of the LOFAR core is $\sim 52.9°$). The right ascension and declination are both given in degrees. The path of the Galactic plane is also shown with a grey line and the location of the Galactic Center (GC) is marked with a cross. The color coding shows the usable length of the data with white signifying an observation that did not process or contained only bad data and black an observation that was fully usable. The length of usable data was determined by subtracting the data that was removed during the single-pulse search from the total integration time of an LPPS observation (see Section 3.3.4 for details).

satellite, which appears in the LPPS data. In our preliminary data reduction runs, zero-DM filtering proved useful as it limits the number of spurious single-pulse detections without negatively impacting the periodicity search results. The pipeline also runs an acceleration search and a single-pulse search on the data, described respectively in sections 3.3.2 and 3.3.3. A full run of the search pipeline produces folded candidate pulsars, plots of the single-pulse detections and some other diagnostic plots that are used to assess the overall data quality.

3.3.2 PERIODICITY SEARCH

EACH of the time-series created by dedispersing the data is run through an acceleration search, in order to increase sensitivity to pulsars whose binary motion induces continuously changing Doppler shifts in the pulse signal. First a power spectrum is created by performing a Fourier transform of the time-series and known bad frequencies are removed from the data using PRESTO's `zapbirds` program. In the case of LPPS data the list of bad frequencies, the so-called "birds list", was created by looking at the results of preliminary survey processing. The most frequently occurring periods of RFI-related candidates were noted and added to the birds list. Often these candidates are visible at multiple DMs because they are narrow-band interference and/or are visible in several or all beams of a particular pointing and/or multiple pointings. The resulting power spectra were corrected for red noise using PRESTO's `rednoise` program and then searched with PRESTO's `accelsearch` routine. An acceleration search compensates for binary motion by applying a matched filter to the spectrum in order to collect spectral power that has been spread over multiple Fourier bins. We performed two searches: one allowing for no drift and one allowing for up to 50 bins of drift in the power spectrum. This number of bins is referred to as z_{max} and corresponds to the maximum number of bins that the highest harmonic of a particular candidate can drift. The maximum binary acceleration that an acceleration search is sensitive to can be calculated using

$$a_{max} = z_{max} \frac{cP}{T_{obs}^2},$$

with c the speed of light in vacuum, P the pulsar period and T_{obs} the observation's integration time (Freire et al., 2005). For a pulsar with a 40-ms period in a relativistic binary LPPS is sensitive up to binary accelerations of $51\,\mathrm{m\,s^{-2}}$. We tested different options to `accelsearch` and settled on using harmonic summing of up to 16 harmonics, harmonic polishing (i.e. an extra step to reject RFI peaks acting as spurious harmonics) and a minimum significance of a pulsar detection of $2\,\sigma$ in the power spectrum.
After all the candidates have been generated for all 7 beams of an LPPS observation, the next step in processing, the candidate selection, begins. For the candidate selection and folding we have two pieces of software. Firstly, there is a Python script that uses parts of PRESTO to sort the pulsar candidates by significance and removes all but the brightest detection of duplicates in period and DM across beams and across z_{max} values. We demand that the effective temporal resolution of the resulting pulse profile is such that we have at least 6 significant bins across the pulse profile. Furthermore we

reject any pulsar candidates with a period below 5 ms (not enough time resolution to achieve an adequate number of profile bins) or above 15 s (there are no known radio pulsars with a period greater than 8.5 s and no known magnetars with a period greater than 12 s) and a DM below 2 pc cm^{-3} (too many spurious detections caused by RFI). After this sifting step all the surviving candidates, with a maximum of 200 candidates per beam, are folded using PRESTO's `prepfold` program and the RFI masks created by the search pipeline. Secondly, there are two neural nets trained on the folds of LPPS pulsar re-detections and RFI instances that help to prioritize the inspection of candidates (for a description of this technique see Eatough et al., 2010).

3.3.3 SINGLE-PULSE SEARCH

THE dedispersed time series are also used to search for single, dispersed bursts. This search is run using the PRESTO `single_pulse_search.py` routine, which employs a box-car match filter to identify individual bursts and creates diagnostic plots. We used box-car lengths of up to 30 bins, making the search sensitive to bursts between 0.655 ms and 19.5 ms at low DMs and, because of down-sampling during dedispersion, to between 41.9 ms and 1.26 s at the very highest DMs. A quick inspection of the data showed that some of the data was badly affected by RFI and could not be processed. After identifying which data sets suffered from this problem and excising bad data (see section 3.3.4) we proceeded with a blind search for single pulses in the remaining data. Those data are then run through a post-processing script that detects significant single pulses. Because PRESTO's `single_pulse_search.py` script, on which our single-pulse search is based, runs on only one trial-DM at a time it detects a single pulse several times (i.e. at several trial-DMs). Our single-pulse post-processing script first associates these detections across trial-DMs, a process we call grouping (see Chapter 5). For each of the groups found in this way the peak signal-to-noise ratio and the DM at which it occurs were determined. After this process, several heuristics are used to find interesting signals. To find bright pulsars we ran the post-processing script demanding that each single-pulse detection (group) had a minimum of 7 members, that it had a minimum signal-to-noise ratio of 8 and that at least 8 such pulses occurred at roughly the same peak DM. For each instance where these criteria were met, a plot was created that was subsequently looked at by a human and followed up if needed, see Figure 3.6 for an example of these plots.

We used the same post-processing script to look for single, dispersed bursts in order to put a limit on bright radio transients (in the absence of strong scattering). We first removed those beams that were known to be bad, rejecting data sets where about 50% or more of the data were bad (for the definition of bad in this context see section

3.3.4). We then searched the data for single dispersed pulses of a signal-to-noise of at least 10 that did not re-occur and were not identified with known pulsars near the beam. We corrected for several factors that are known to affect the sensitivity of each observation: zenith angle dependence of LOFAR sensitivity, number of (sub-)stations available and integration time differences caused by bad data.
The sensitivity of the LPPS beam as a function of zenith angle is shown in Figure 3.4. In our calculations we used the half power point of the beam as a cut-off for the beam footprint. To model the projected baseline's effect on the beam shape we used a factor $1/\cos\alpha$, where α is the zenith angle of the beam center, to elongate the LPPS beams away from zenith. For the integration time of each observation we used the fraction of good data previously identified (see Section 3.3.4). We calculated a gain for each LPPS observation using Eq. 3.1 and the gain we derived from the periodicity search (see Section 3.4.4). We report the results of this analysis and the resulting full-sky rate of bright radio transients at LOFAR's observing frequencies in section 3.4.6.

3.3.4 DATA QUALITY ISSUES

SINCE LPPS data were taken quite early during LOFAR's commissioning period data quality issues were expected, and soon found. Many of the stations used in the LPPS observations had just barely been brought online and in some cases the hardware had not yet been fully validated. This meant that not only were the stations not yet calibrated for internal cable delays (necessary to achieve the full-station sensitivity when the antenna elements are combined into a station beam), there were also several faulty elements in need of repair or proper installation. In the case of an incoherent sum of station beams, as used for LPPS, a single malfunctioning station can significantly affect the quality of the incoherent array beam and the observed RFI can be dominated by these internally generated effects. Consequently, a significant fraction of the data could not be processed using the standard PRESTO tools and another fraction of the data, while processable, was too badly affected by RFI to be useful. We stopped processing any data set where one of the beams was corrupted. With the stations now properly calibrated and with better system health monitoring in place, the data quality of current LOFAR data is *much* improved.
For the periodicity search we relied on the combination of a so-called "birds" list[6], PRESTO's candidate selection, and two neural nets that were trained on LPPS pulsar re-detections during earlier, partial processing runs (to keep the number of pulsar

[6]Spurious frequencies in the power spectra known not to be pulsars because they are detected in several observations at different DMs and sky positions.

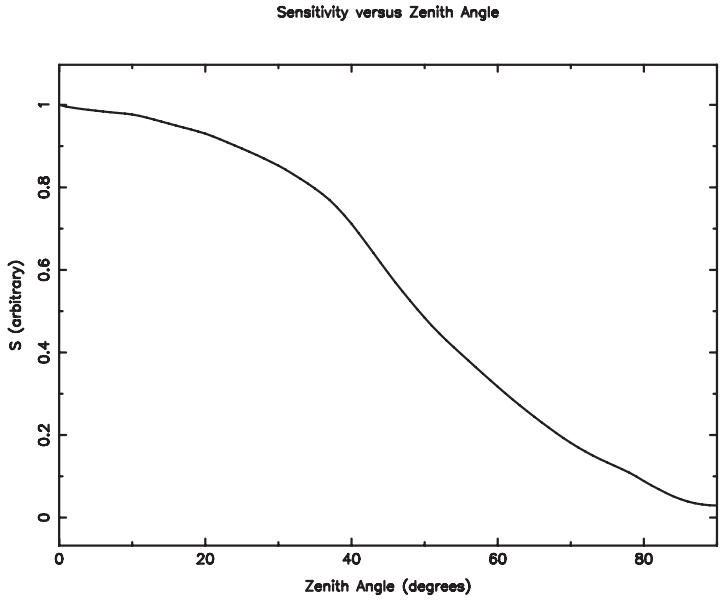

Figure 3.4: The sensitivity of LPPS as a function of zenith angle. This function is the result of a full-wave EM antenna simulation for the LPPS frequency range, over a 3x3-tile section a LOFAR HBA station (Wijnholds et al., 2012).

candidates manageable). In the single-pulse search we found that RFI or even bright pulsars that produce many single-pulse candidates could overwhelm the standard diagnostic plots created by PRESTO. We developed a condensed version of the single-pulse diagnostic plots where the single-pulse candidates are not individually drawn but shown as a 2 dimensional, color-coded, histogram on the time-DM plane (see Section 5.3.1). Figure 3.5 shows an example of such "condensed" single-pulse plots for a data set with 2 pulsars and a large amount of RFI. We further created a heuristic to identify bad data in the single-pulse search results: if more than 500 single-pulse candidates across all DM trials were detected in 10-s blocks of data, then we considered them bad. The threshold was determined by inspecting the condensed plots made for an earlier processing of one third of the LPPS data. Using this heuristic we cleaned up the data and were able to estimate the effective exposure time for each LPPS beam. For the limit on fast transients we rejected any data set that contained bad data for about 50%

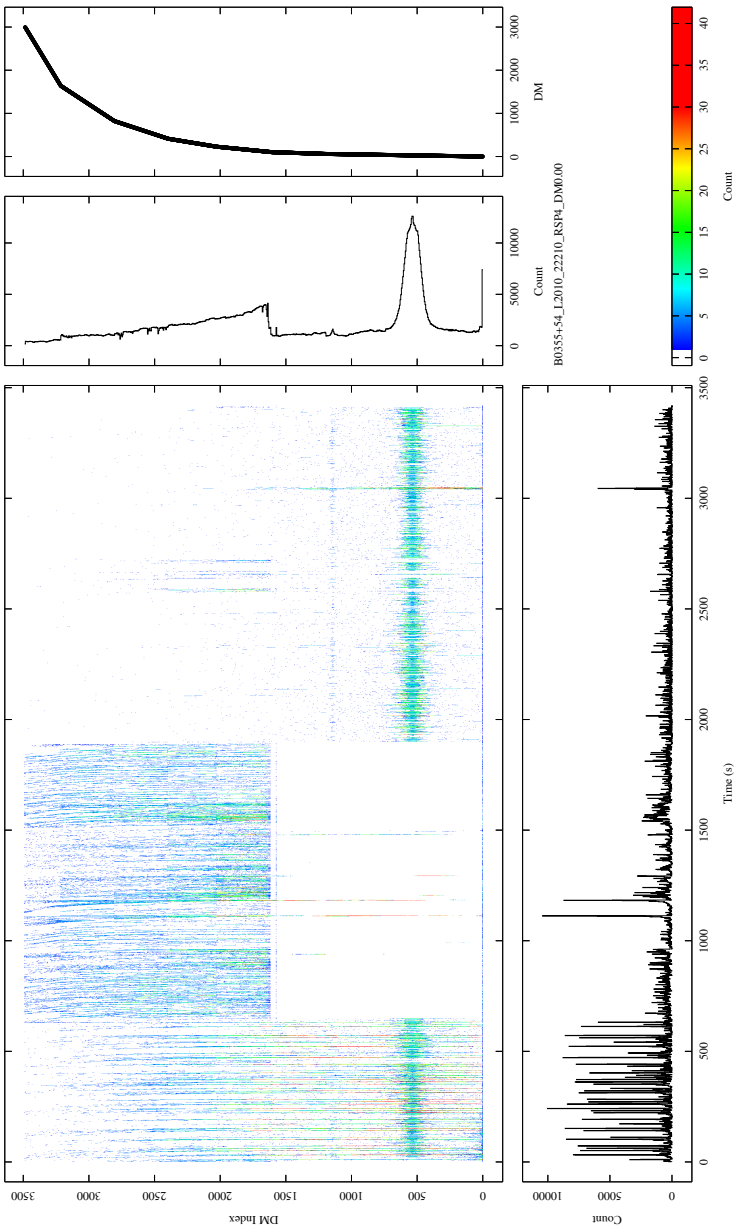

Figure 3.5: An LPPS pointing afflicted by strong RFI and containing two pulsars, B0329+54 and B0355+54, plotted using our custom "condensed" single-pulse plotter. The two pulsars have DMs of 26.8 pc cm^{-3} and 57.1 pc cm^{-3}, respectively, and are visible through their many single pulses forming horizontal bars at DM indices of about 550 and 1100, respectively. The main panel of this figure shows the color-coded number of single-pulse detections binned in time (1 second per cell) and across trial DMs (5 DM trials per cell). The panels to the right and to the bottom of the main panel show histograms created by respectively collapsing over time and over the trial-DMs. The right-most panel shows how the trial-DM number to real DM value (in pc cm^{-3}) mapping.

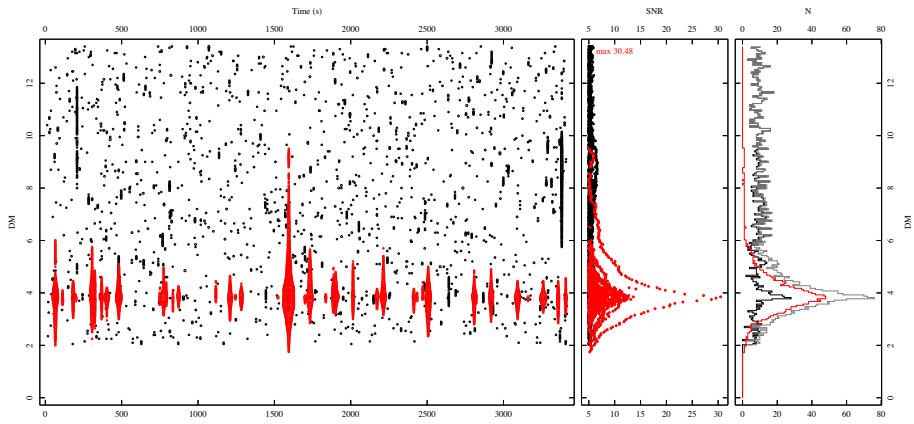

Figure 3.6: A detection plot of PSR J0242+6256, as produced by our single-pulse post processing scripts. The pulsar is visible in the main DM versus time panel as a series of individual pulses with a DM$\sim$ 3.9 pc cm^{-3}. During this observation the pulsar emitted one very bright pulse of a signal-to-noise ratio of about 30, visible at near 1600 s into the observation. Our automated pulse grouping algorithm (see Chapter 5) has colored events that are judged to be of an astrophysical origin in red (the black points were automatically judged to be either statistical noise or RFI). The two panels on the right show the events collapsed in time (i.e. accumulated over the whole observation) as a function of cumulative signal-to-noise ratio and number of events, respectively.

or more of the observation time. To make sure we did not miss detections of bright pulsars because they crossed the 500 candidates per 10 s threshold, we inspected the condensed single-pulse plots for all data sets.

3.4 RESULTS

3.4.1 PERIODICITY SEARCH RESULTS

No previously unknown pulsars were discovered in LPPS — although not all pulsars detected had been previously published in the refereed literature. In total, the periodicity search of LPPS data yielded the re-detections of 54 pulsars. A later verification of all undetected pulsars with an ATNF catalog (Manchester et al., 2005) 400-MHz flux above 6 mJy yielded the re-detection of a further 9 pulsars (see Section 3.4.3). In Table 3.1 we list the pulsars re-detected through the blind periodicity search,

as well as those detected by performing direct folds on the data and those detected through the single-pulse search. The profiles for the pulsars detected by the periodicity search and the direct folds are shown in Figure 3.7, 3.8 and 3.9. Figure 3.10 shows a histogram of the distances of the detected pulsars to the center of the beam in which they were identified. Beyond the re-detection of 51 pulsars already listed in the ATNF pulsar catalog, we found 3 pulsars not yet included there; see Section 3.4.2 for more details.

Table 3.1: All pulsars detected in the LPPS data. Sources marked with an asterisk were used to derive an estimate for the LPPS gain (see section 3.4.4). The column headed by an M (method) lists how the pulsar was detected — through a periodicity search (p), through a direct fold using a known ephemeris (d), or through single-pulse searches (s). The next column, headed by α, lists the distance to the beam center in degrees at which the pulsar was detected (based on the ATNF pulsar database positions). The *DM* and *period* columns lists the values as reported by PRESTO after folding the data on the known ephemeris using 256 bins. The next two columns report the *peak* and the *cumulative* signal-to-noise ratio derived from the pulse profiles. For profiles where no flat baseline could not be determined, no numbers are given for these signal-to-noise ratios. The last column shows the peak signal-to-noise ratio of the brightest pulse found in the *single pulse search* as reported by PRESTO (not corrected for zero-DM filtering).

Pulsar	M	α	DM	Period (ms)	S/N_p	S/N_{cum}	S/N_s
B0045+33	p	1.53	39.940	1217.0955(20)	14.4	-	-
B0105+65	d	1.99	30.460	1283.6642(18)	9.0	93.3	-
B0136+57*	p	2.57	73.779	272.45744(15)	7.1	74.3	-
B0138+59*	p,s	2.67	34.797	1222.9487(16)	9.1	29.3	6.78
B0144+59	d	1.61	40.111	196.321764(92)	6.6	64.5	-
B0154+61	s	1.37	30.00	-	-	-	9.09
J0242+6256	p,s	-	3.903	591.73821(58)	9.0	36.6	30.53
B0329+54*	p,s	2.44	26.833	714.518368(26)	605.6	2137.7	-
B0355+54*	p,s	1.10	57.142	1.56.384421(44)	31.5	352.5	7.40
B0402+61	p	1.65	65.303	594.57621(42)	7.6	82.4	-
B0450+55*	p	2.20	14.495	340.72979(19)	31.8	237.9	-
J0540+3207	p	-	62.371	524.28512(34)	8.8	-	-
B0523+11	p	0.85	79.345	345.43894(21)	7.6	149.4	-
B0611+22*	p	1.53	96.910	334.99008(27)	10.1	208.7	-
B0626+24	d	2.03	84.195	476.623636(24)	4.5	35.7	-
B0655+64*	p	0.59	8.771	195.670990(21)	81.5	550.8	-
B0809+74	s	2.66	5.75	-	-	-	14.08
B0823+26*	p,s	1.66	19.454	530.660885(92)	120.4	560.9	22.16
B0834+06*	p	1.50	12.889	1273.77231(20)	226.7	347.9	-
B0917+63	p,s	0.50	13.158	1567.9958(18)	20.2	243.9	10.88
B0919+06*	p	2.09	27.271	430.62707(11)	92.9	618.1	-
B0950+08*	p,s	2.23	2.958	253.065052(26)	60.1	658.2	21.18
B1112+50	p,s	1.68	9.195	1656.4379(18)	-	-	24.26
B1237+25*	p,s	1.92	9.242	1382.4498(13)	27.1	46.5	30.89

Table 3.1: Continued

Pulsar	M	α	DM	Period (ms)	S/N_p	S/N_{cum}	S/N_s
B1322+83	p	1.61	31.312	670.03774(66)	7.3	-	-
B1508+55*	p	2.10	19.613	739.684995(57)	303.1	1451.4	-
B1530+27	p,s	1.41	14.698	1124.8361(21)	-	-	10.47
B1541+09*	p	1.67	35.240	748.44609(70)	26.0	247.0	-
B1604−00	p	2.70	10.682	421.81626(50)	-	-	-
B1633+24	p	1.73	24.320	490.50603(45)	-	-	-
J1758+3030	p	1.33	34.900	947.2572(14)	-	-	-
B1811+40*	p	0.94	41.487	931.09033(92)	30.1	309.6	-
B1821+05*	p	1.65	66.775	752.90407(73)	25.1	192.6	-
B1839+09	p	0.75	49.107	381.32032(35)	12.1	-	-
B1839+56	p	2.58	26.298	1652.8627(45)	-	-	-
B1842+14*	p	1.55	41.510	375.45373(19)	29.8	147.3	-
B1905+39*	p,s	1.55	30.960	1235.7613(14)	11.9	38.7	11.61
B1918+26	p	0.39	27.620	785.52187(83)	18.1	136.3	-
B1919+21	p,s	2.39	12.455	1337.30910(34)	-	-	31.67
B1929+10	p	2.14	3.180	226.517770(82)	-	-	-
B1949+14	d	1.44	31.460	275.02609(13)	3.6	39.1	-
B1951+32	d	0.54	45.006	39.534014(26)	7.7	223.2	-
B1953+50*	p,s	1.29	31.974	518.93973(38)	28.4	96.5	11.88
B2016+28*	p,s	0.72	14.172	557.95324(13)	124.6	156.6	13.75
B2020+28*	p	0.43	24.640	343.403254(68)	50.9	314.8	-
B2021+51*	p,s	0.71	22.648	529.19960(54)	18.2	182.9	30.04
B2022+50*	p	1.64	33.021	372.62092(29)	9.7	28.7	-
J2043+2740*	p	1.42	21.000	96.131283(26)	22.2	276.6	-
B2110+27	p	2.95	25.113	1202.8533(14)	36.8	199.4	-
B2111+46*	p,s	1.66	141.260	1014.6865(18)	24.5	483.9	11.88
J2139+2242	p	0.79	44.100	1083.5142(18)	11.1	114.5	-
B2154+40	p	2.09	70.857	1525.2648(56)	-	-	-
B2217+47*	p,s	1.80	43.519	538.470628(26)	446.6	1976.5	12.14
B2224+65*	p	2.86	36.079	682.54774(52)	7.7	55.8	-
B2227+61	d	0.71	124.614	443.05771(24)	5.0	178.7	-
B2255+58	p	1.26	151.082	368.24980(12)	-	-	-
J2302+6028	d	2.20	156.700	1206.4053(11)	6.0	76.9	-
B2303+30	p	1.14	49.544	1575.88880(29)	-	-	-
B2306+55*	p	2.75	46.538	475.06987(20)	5.0	13.4	-
B2310+42*	p	1.78	17.276	349.43375(20)	25.0	215.5	-
B2315+21	p	2.11	20.906	1444.6561(25)	22.8	-	-
J2317+68	p	-	71.156	813.37167(70)	7.1	35.6	-
B2319+60	d	1.75	94.591	2256.4395(34)	2.4	-	-
B2334+61*	p,s	2.14	58.410	495.38600(46)	10.8	90.2	13.11
B2351+61	d	0.15	94.662	944.79253(78)	9.9	-	-

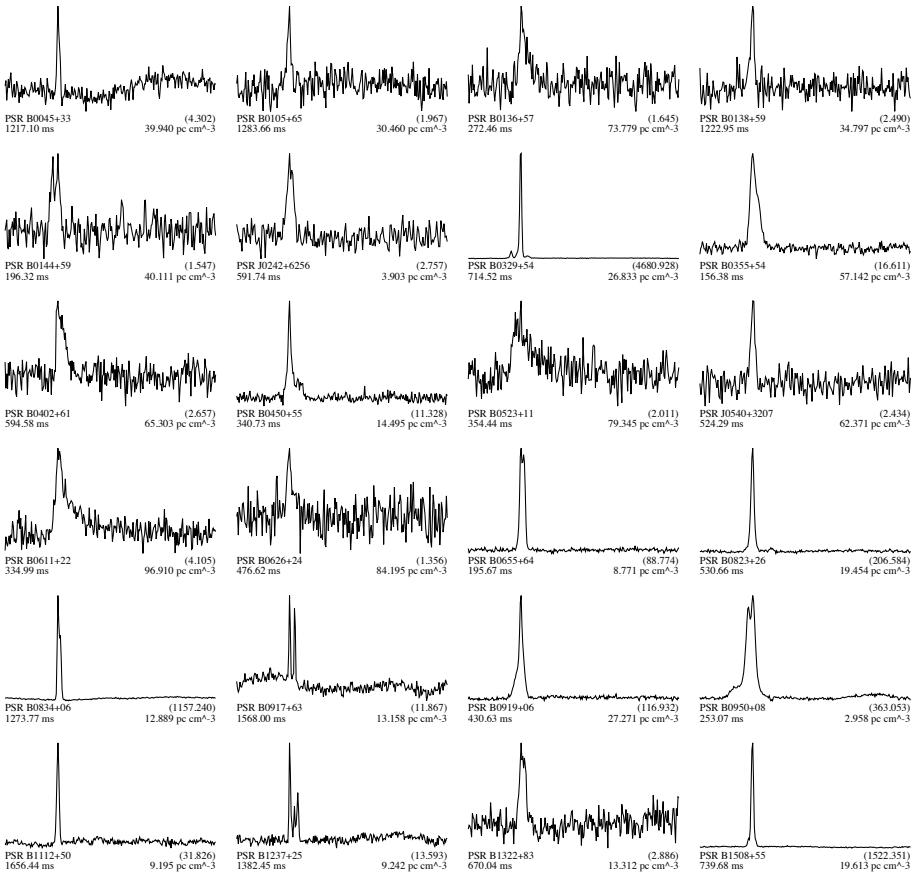

Figure 3.7: LPPS pulsar profiles, page 1. For each pulsar, the catalog name, detected pulse period, detected DM, and reduced chi-squared significance from the automated search fold are given. One full rotational cycle is show. Some of the brightest pulsars were detected multiple times; only the highest signal-to-noise detection is shown here. Several of the pulse profiles show scattering tails, e.g. PSRs B0523+11, B0611+22, B2111+46, making them excellent sources for studies of the interstellar medium. In many cases the off-pulse baseline is not flat due to strong RFI that could not be completely excised.

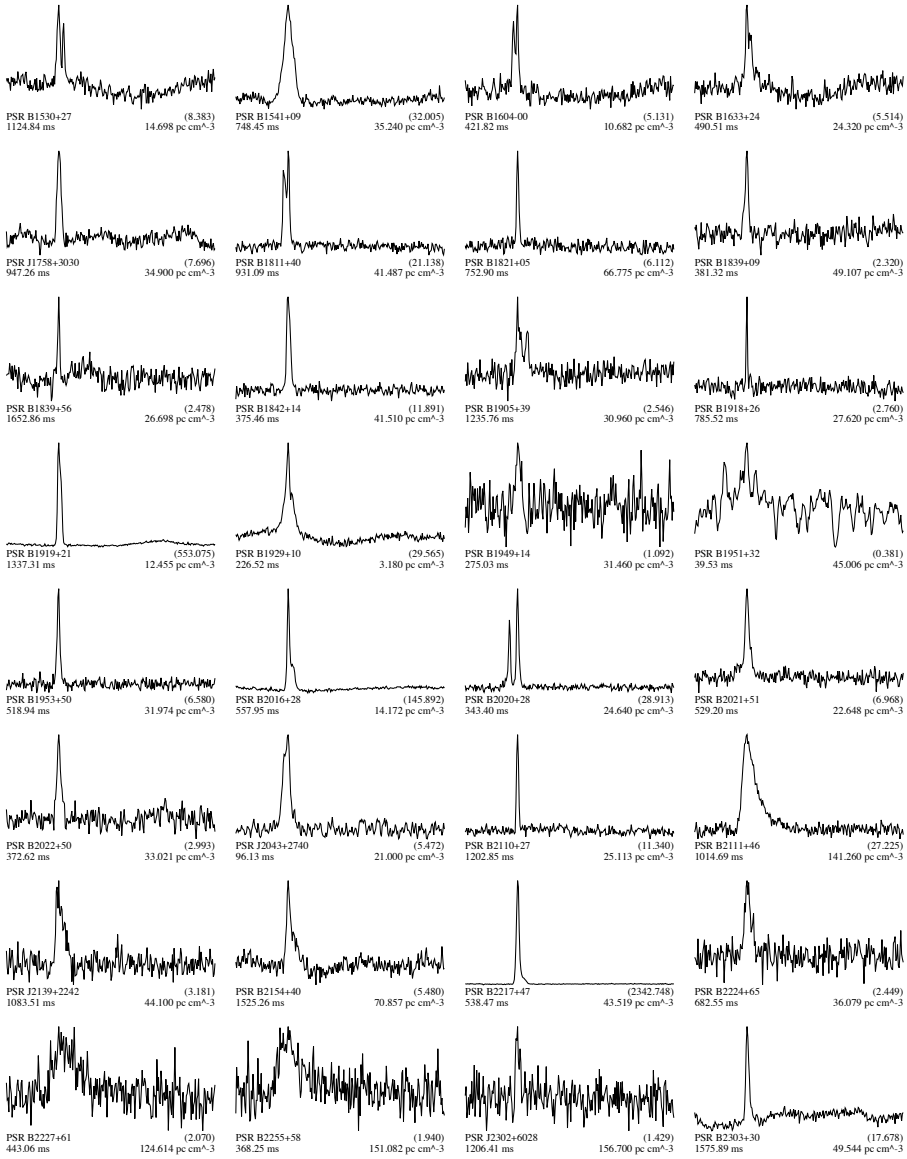

Figure 3.8: LPPS pulsar profiles, page 2.

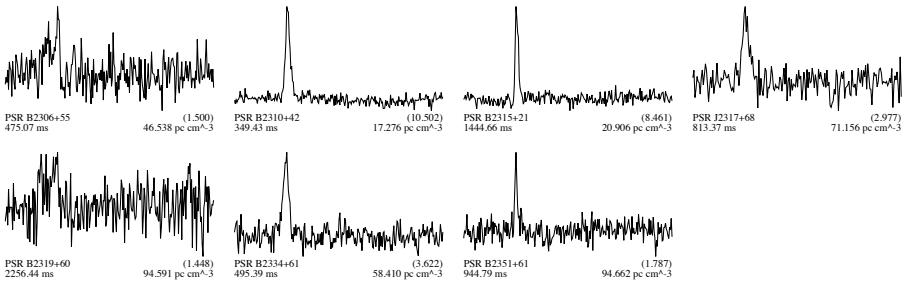

Figure 3.9: LPPS pulsar profiles, page 3.

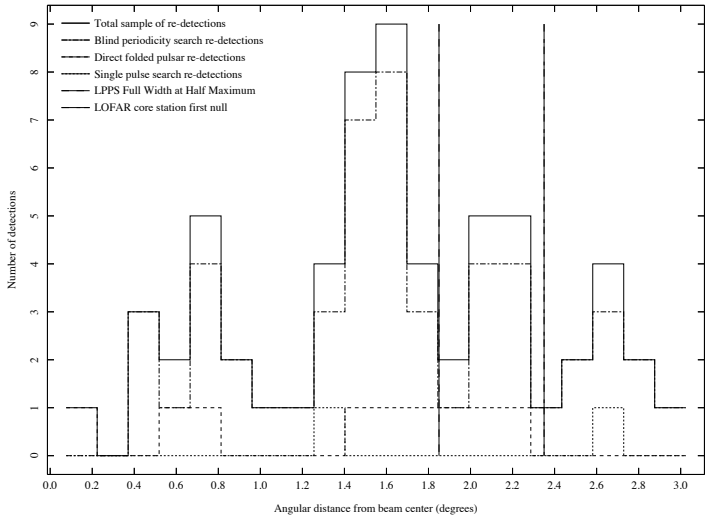

Figure 3.10: Histogram of the angular offsets between the detected pulsars and the nearest beam center (based on ATNF pulsar catalog positions; Manchester et al., 2005) Shown are the 51 pulsars re-detected in the periodicity search, 9 pulsars re-detected by folding on known ephemerides and 2 pulsars only detected in the single pulse search.

3.4.2 UNPUBLISHED OR PARTIALLY PUBLISHED SOURCES

As mentioned in section 3.4.1, all detected pulsars were previously known, but not all had been published before in the refereed literature. These three we describe in some more detail below.

PSR J0242+6256

The pulsar J0242+6256 is a low-luminosity, low-DM pulsar, which was discovered by the GBT350 Survey of the Northern Galactic Plane for Pulsars and Transients (Hessels et al., 2008). In that proceedings article it is known as PSR J0240+62 — in Chapter 4 we more precisely determined its position so we refer to it here as PSR J0242+6256. In LPPS, it was detected both in the periodicity and single pulse search. The single-pulse discovery observation (Fig. 3.17) already made clear that PSR J0242+6256 has a broad pulse-energy distribution and occasionally produces a very bright pulse. In many ways this source is a prototype for the nearby, low-DM, perhaps intermittent, sources that LOFAR is best equipped to discover.

In a 1-hr follow-up observation taken with the full LOFAR HBA core and 78 MHz bandwidth, i.e. at a far higher sensitivity than the discovery plot, the large pulse-to-pulse intensity variations in J0242+6256 become even more clear. In Fig. 3.11 we show that some bright bursts outshine the average pulse by a factor 25. In most of the well-studied pulsars this ratio is much lower (e.g., a factor of only 2 in PSR B0809+74; van Leeuwen et al., 2002). It is only higher in RRATs and PSR B0656+14 (where it is of order 100; Weltevrede et al., 2006c). The on-pulse window of the full observation is shown in Fig. 3.12. Using LOFAR's multi-beaming this observation was also used to get a better determination of the position, as described in more detail in Chapter 4.

PSR J0540+3207

Pulsar J0540+3207 is a 2004 Pulsar Arecibo L-Band Feed Array (PALFA) survey discovery that was detected in LPPS data through the periodicity search. In Cordes et al. (2006) this 524-ms pulsar is reported at a DM of 120 pc cm^{-3}, while our detection firmly puts it at 62 pc cm^{-3} – a value independently confirmed by the recent publication of a full timing solution for this pulsar by Nice et al. (2013).

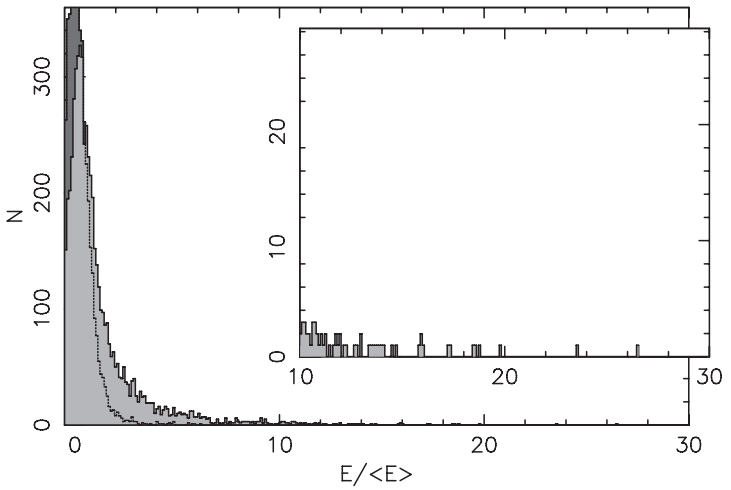

Figure 3.11: Pulsar energy histogram for PSR J0242+6256. Shown are the individual pulse energies for 6000 pulses, compared to their average. The dashed line, filled in dark gray, represents the off-pulse noise distribution. The light gray histogram is the energy present in the on-pulse region (Fig. 3.12). That distribution peaks near zero and has significant overlap with the background histogram. In those pulses no pulsar emission is detected.

INDEPENDENT DISCOVERY PSR J2317+68

THE most genuinely 'new' source in LPPS is PSR J2317+68, a 813-ms pulsar at a DM of 71.158 pc cm^{-3}, which we *independently* discovered. This source had only months earlier been discovered in the GBNCC at 350 MHz (Stovall, private communication). This independent discovery shows that even an uncalibrated early version of LOFAR is already competitive with the state-of-the-art pulsar searches conducted using the largest steerable dish radio telescope in the world.

3.4.3 DIRECTLY FOLDED PULSARS

AS a check on the performance of our pulsar search we investigated whether all previously known pulsars within the survey area were in fact re-detected in LPPS. We selected from the ATNF catalog all pulsars in the northern hemisphere and

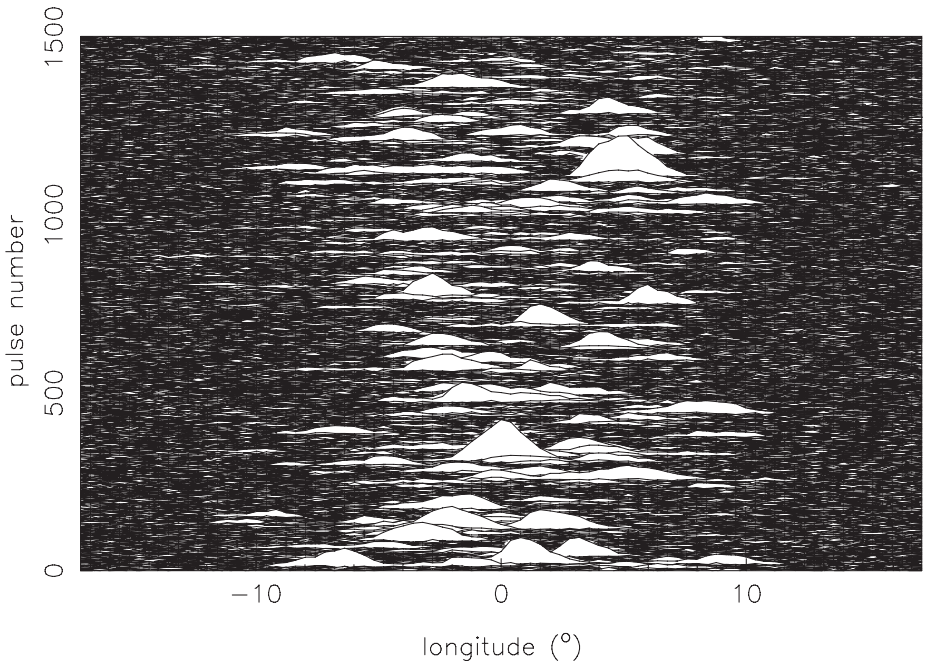

Figure 3.12: A 1500 s section of data from a 1-hour observation of PSR J0242+6256. Only the on-pulse window is shown. A large variation in pulse intensities is visible.

determined in which LPPS beam they should have been observed. If the pulsar fell in an un-processable observation or an observation that was badly affected by RFI we determined the next closest beam that was of sufficient quality (if there was such a beam within 5 degrees from the pulsar). We then checked those pulsars which also had a determined 400-MHz ATNF flux over 6 mJy. For each pulsar that met these criteria we folded the data directly (i.e. without running a blind search) on the known ephemeris and checked whether it was visible. This process led to the detection of a further 9 pulsars not picked up by the periodicity search. These are tabulated in 3.1. Of these pulsars, 3 were quite bright and present in a relatively RFI-clean data set. These sources seemingly should have been detectable, but were not. It is possible that they did not survive the candidate sifting process or were not identified by the neural network. It is also possible that the presence of strong red-noise in the power spectra masked their signal during the search process. The other 6 pulsars found through direct folds and manual inspection were less bright and present in less clean data. It

is thus likely that they were missed because of RFI contamination (or an internal system problem). These latter pulsars quite often lacked well-defined signal-to-noise as function of DM curves (a major discriminator between promising candidates and RFI). In 2 cases the detections are so weak that without prior knowledge of their presence they would have been rejected during manual inspection.

3.4.4 POST FACTO GAIN DETERMINATION

THE LPPS survey was taken in December 2010, when LOFAR was not yet fully calibrated. Determining the absolute fluxes for our re-detections is therefore highly uncertain and we did not attempt it. We did however attempt to derive the gain for LOFAR observing in the LPPS configuration, to get a first-order indication of the sensitivity of LOFAR for pulsar surveying in this mode.

For reference, we first derive the assumed ideal thermal-limit performance and then the gain $G = \frac{A_{eff}}{2k}$, where A_{eff} is the effective area and Boltzmann's constant $k = 1.38 \times 10^{-23}\,\mathrm{W\,s/K} = 1.38 \times 10^{3}\,\mathrm{Jy\,m^2/K}$. For the core stations, the reported[7] effective area A_{eff} is 600 $\mathrm{m^2}$; for the remote stations it is 1200 $\mathrm{m^2}$. Thus their respective gains are G_{core}=0.21 K/Jy, G_{remote}=0.42 K/Jy. For our maximum sensitivity, the incoherent sum of 38 core and 6 remote stations, the scaling from Eq. 3.1 then produces a theoretical gain of G=1.6 K/Jy.

To determine the actual gain at the time of LPPS, we used a slightly modified version of the radiometer equation. Starting from Bhattacharya (1998, Eq. 2, p. 108) we write the flux S_i of the i-th profile bin

$$S_i = \frac{\beta_i}{G} \frac{T_{\mathrm{rec}} + T_{\mathrm{sky}}}{\sqrt{N_{\mathrm{pol}} \mathrm{BW} \tau}} \sqrt{N_{\mathrm{b}}}, \tag{3.2}$$

with G the telescope gain, T_{rec} the receiver temperature, T_{sky} the sky temperature, n_{pol} the number of polarizations, BW the observational bandwidth, τ the integration time and N_{b} the number of profile bins. Instead of then using the peak signal to noise and the pulse width to arrive at an expression for the average flux S_{avg} we determine it directly by averaging over S_i

$$S_{\mathrm{avg}} = \frac{1}{N_{\mathrm{b}}} \sum_{i=1}^{N_{\mathrm{b}}} S_i = \frac{T_{\mathrm{rec}} + T_{\mathrm{sky}}}{G\sqrt{N_{\mathrm{pol}} \mathrm{BW} \tau}} \frac{1}{\sqrt{N_{\mathrm{b}}}} \sum_{i=1}^{N_{\mathrm{b}}} \beta_i = \frac{T_{\mathrm{rec}} + T_{\mathrm{sky}}}{G\sqrt{N_{\mathrm{pol}} \mathrm{BW} \tau}} \frac{\beta_{\mathrm{cum}}}{\sqrt{N_{\mathrm{b}}}}. \tag{3.3}$$

[7] "Sensitivity of the LOFAR array", http://www.astron.nl/radio-observatory/astronomers/lofar-imaging-capabilities-sensitivity/sensitivity-lofar-array/sensiti

In this equation $\beta_{\rm cum}$ is the cumulative signal-to-noise ratio. By now comparing the ATNF 400-MHz fluxes scaled to the LPPS observing band (assuming no spectral turnover) with the uncalibrated fluxes determined from the radiometer equation we can determine the gain. For all LPPS observations[8] $T_{\rm rec}$ is 140 K (van Leeuwen & Stappers, 2010), $T_{\rm sky}$ can be determined by scaling the sky temperature at 408 MHz from Haslam et al. (1982) to the LPPS band using the $T \propto \nu^{-2.6}$ power-law from Lawson et al. (1987), $n_{\rm pol}$ is 2, BW is 6.8 MHz, τ is 57 minutes.

We used the 50 blind-search re-detections that had an available 400-MHz flux in the ATNF catalog. Because we found a dependence on $N_{\rm b}$ of $\beta_{\rm cum}$ we re-folded all pulsars in our sample to an $N_{\rm b}$ of 256 bins. From this sample we removed 5 pulsars that were in observations significantly affected by RFI, 14 pulsars whose folds had ill-determined baselines (i.e. a non-flat off-pulse region) and 1 pulsar whose cumulative signal-to-noise ratio could not be determined by our scripts. For the remaining sample of 30 pulsars we assumed that the scatter around the mean spectral index of -1.8 (Maron et al., 2000), the error on $T_{\rm sky}$, the error on $\beta_{\rm cum}$, possible scintillation during the LOFAR observation and the error on the cataloged flux are random and thus do not bias the uncalibrated flux values found for the LPPS detections. If many of these sources have a spectral turnover between $140-400$ MHz then this will systematically bias the inferred gain to be lower.

Most LPPS observations were taken towards the zenith, so we used the beam model shown in Figure 3.1 and the zenith angle dependence model shown in Figure 3.4, both in tabulated form, to correct all derived pulsar fluxes for these effects. The beam model was applied to the angles between the beam center and the pulsar, with no correction for beam elongation. Because LOFAR was being extended during the LPPS observing run, not all observations used the same number of stations: we corrected for that using Eq. 3.1. Comparing the catalog fluxes with the uncalibrated fluxes we found in LPPS allowed us to derive a maximum gain[9] for each of the 30 included pulsar detections (see Figure 3.13). Taking the average we thus find the maximum gain for an observation (zenith, using 38 core and 6 remote stations) to be $G = 0.60 \pm 0.13$ K/Jy. This gain estimate shows that we have been able to reach an appreciable fraction ($\sim 40\%$) of LOFAR's full sensitivity using just the uncalibrated array of December 2010. Performing this calculation for a different number of bins yields slightly different values of the gain, going up slowly with the number of bins in the profile. The values found for the gain using 64, 128, 256, 512 and 1024 bins are compatible within the calculated errors. We speculate that the upward trend is

[8] "Sensitivity of the LOFAR array", `http://www.astron.nl/radio-observatory/astronomers/lofar-imaging-capabilities-sensitivity/sensitivity-lofar-array/sensiti`

[9] Because the corrections we described above effectively put the pulsar towards the zenith.

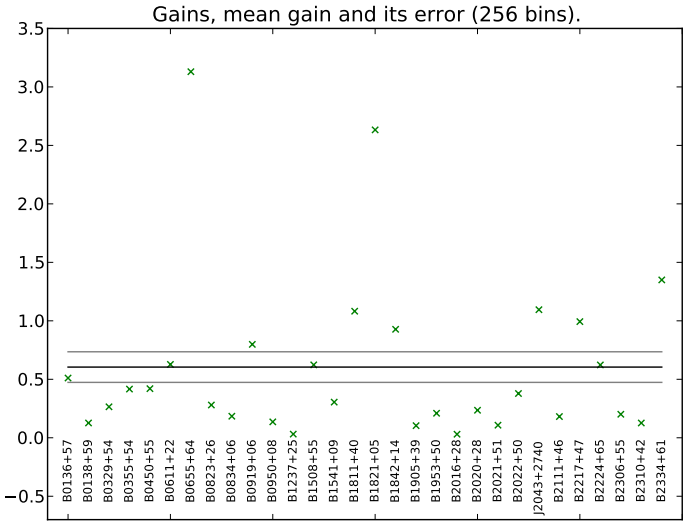

Figure 3.13: The derived gains for each of the pulsars, and the determined average gain for LPPS. The black line signifies the mean gain and the gray lines the errors on the determination (error e calculated as $e = \sigma/\sqrt{n}$ with σ the standard deviation and n the number of pulsars).

caused by profile bins no longer being independent from each other (starting from 2 profiles where that is true at 256 bins increasing to 19 profiles at 1024 bins). Another possibilty is that the presence of non-Gaussian RFI affects the determination of the cumulative signal-to-noise ratio from the average pulse profiles.

3.4.5 SINGLE-PULSE SEARCH RE-DETECTIONS

THE fast transients search resulted in 20 pulsar re-detections, also tabulated in Table 3.1. Of these pulsars 18 were detected in the final processing and two, B0154+61 and B0809+74, resulted from earlier partial processing. One source, PSR J0242+6256, stands out for appearing particularly bright in the LOFAR band. Figure 3.17 shows one detection of this pulsar in LPPS observation L2010_21756. The extremely bright pulsar B0329+54 was detected in the side lobes for many observations; Figure 3.14 shows B0329+54 detected 109 degrees away from the pointing center of the observation.

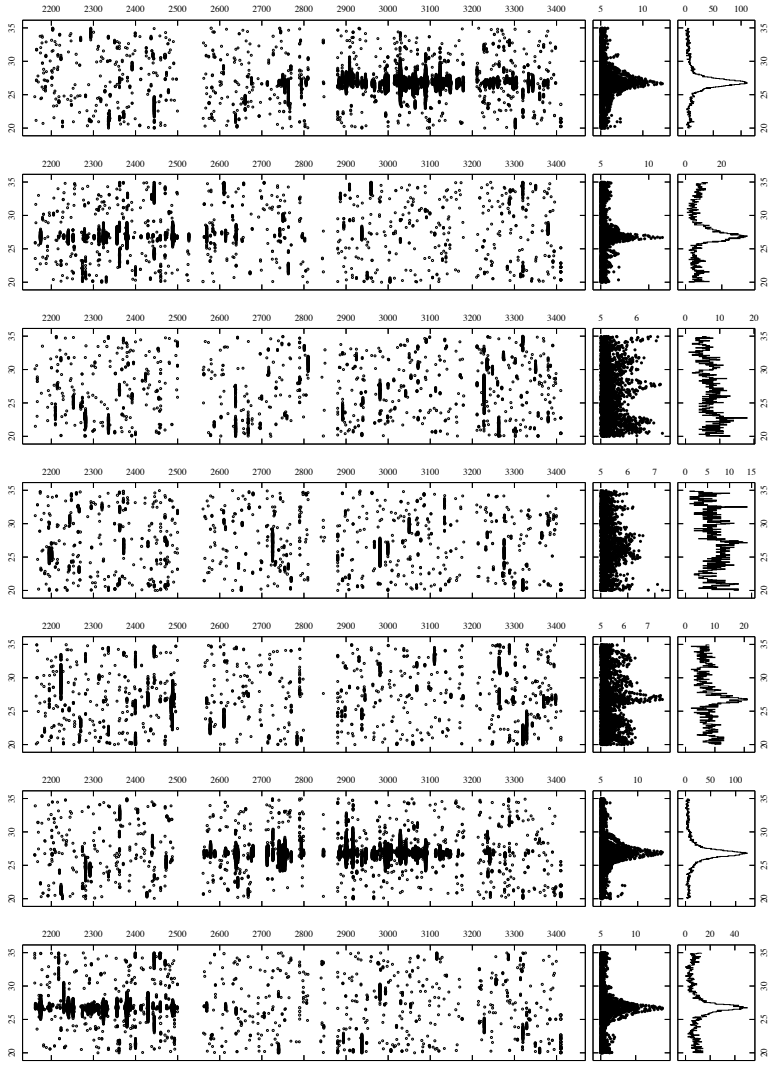

Figure 3.14: Pulsar B0329+54, detected 109 degrees from the central beam of an LPPS survey pointing. The pulsar appears to jump between beams because it is passing through the side-lobes for that observation.

3.4.6 LIMIT ON THE RATE OF FAST TRANSIENTS

THE detection of a bright, highly dispersed radio burst of apparent extra-galactic origin was first reported by Lorimer et al. (2007) and further detections have since been reported by Keane et al. (2011) and Thornton et al. (2013). To date all detections of this type of burst were achieved using the Parkes telescope, at 1.4 GHz. As the LPPS survey uses long observations with large FoVs, the survey data can be used to either detect such bursts, or to derive a limit on the rate of bright dispersed radio bursts at low radio frequencies (in the absence of strong scattering).

We used our single-pulse search post-processing scripts to search the data down to a signal-to-noise ratio of 10 at a DM higher than 2 cm^{-3} pc, because at lower DMs the data was particularly affected by RFI. Through visual inspection of all pulses that crossed this threshold, chosen to be unambiguously higher than the noise background observed in the data, we were able to associate them all with either a known pulsar or RFI (as visible by detections across multiple beams or across multiple trial DMs).

The resulting fast-transient limit then depends on the telescope sensitivity, and sky coverage in both time and area. We define the sky coverage as being out to the FWHM of each beam and the time coverage as the amount of observing time that was determined to be uncontaminated in Section 3.3.3.

Since LOFAR was not yet fully calibrated we use the gain derived from the LPPS pulsar re-detections as described in Section 3.4.4 for our sensitivity calculations. For each LPPS observation, and on a per-beam basis, we determined the zenith angle and through that the beam size and sensitivity. Furthermore, we determined the integration time by noting how much data we had removed in the thresholding step described in Section 3.3.4. The gain as derived in Section 3.4.4 is the gain at the beam center, so for our present purposes we multiply it with 0.73 to find the gain averaged over the LPPS beam FoV. We use this *average* instead of the *minimum* gain over the FoV (which would be the gain at FWHM) to be able to compare our result to those of other surveys which also use this average (e.g. Edwards et al., 2001). We derived a flux limit for each of the beams using a $T_{\rm sys} + T_{\rm sky}$ of 500 K. Figure 3.15 shows a histogram of the flux limits determined on a per beam basis. We removed from consideration any beam with a flux limit above 200 Jy. This removal is justified by noting that their low sensitivity is likely caused by RFI and/or calibration issues and the fact that their sensitivities clearly are in the tail of the flux limit distribution. After this removal we arrived at an average flux limit of 107 Jy at LPPS observing frequencies and a rate limit for bursts brighter than that of no more than 1.5×10^2 bursts per day.

In Fig. 3.16 we compare this rate to the extrapolated occurrence based on the detection of the first two “Lorimer” bursts (now also called “fast radio bursts" or “FRBs"),

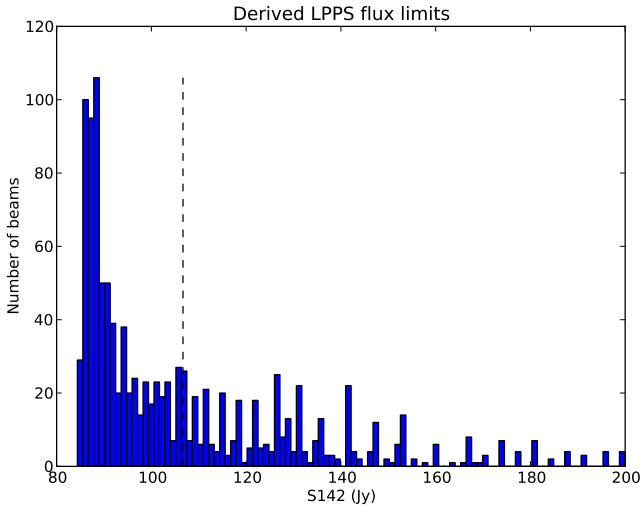

Figure 3.15: Histogram of S_{min} values derived for each LPPS beam. Based on the non-detection of pulses with a SNR of more than 10. The dashed line shows the average flux limit for all non-rejected beams. The derivation of these flux limits is described in 3.4.4.

and limits set by other surveys. These other surveys were all performed at higher frequencies, 270–1400 MHz. The low observing frequency used in LPPS means that any steep spectrum sources would appear much brighter, and consequently that a flux limit obtained with LOFAR would be much more constraining when extrapolated to higher observing frequencies. The original detection of the Lorimer burst had a steep spectrum with a determined spectral index of −4 (Lorimer et al., 2007), while one of the recently detected bursts reported on in (Thornton et al., 2013) showed no such steep spectrum but instead had 100 MHz wide bright bands (at L-Band). Given our limited knowledge at this time, we have not corrected the LPPS rates for either effect.

3.4.7 COMPARISON TO RECENT LOW-FREQUENCY OR WIDE-FIELD SURVEYS

TWO features that make LPPS stand out from other recent pulsar survey efforts (e.g. the Parkes multi-beam pulsar survey, Manchester et al. 2001; the GBT driftscan survey,

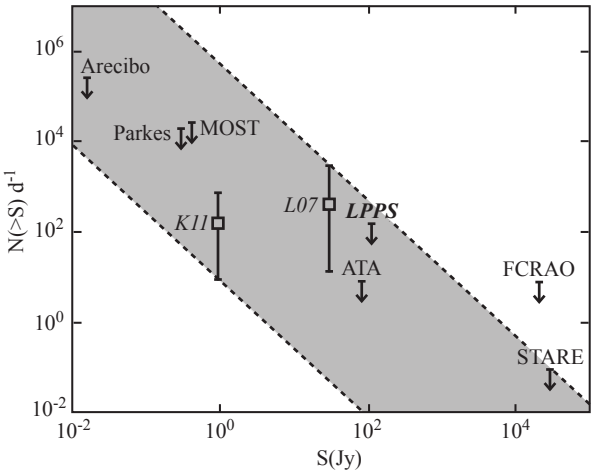

Figure 3.16: The limits on transient occurrence per day N versus flux S, on a logarithmic scale, comparing fast-transient surveys carried out previously (Kulkarni et al., 2008) with LPPS. The two first extragalactic bursts (Lorimer et al., 2007; Keane et al., 2011) are plotted with their errors. Thornton et al. (2013) derive a compatible rate. The area between the dashed lines represents the $N(>S) \propto S^{-3/2}$ prediction from a homogeneous, stationary population of objects. The LPPS limit is seen near the center.

Boyles et al. 2013), are the very low observing frequency and the large dwell time. Below we thus compare the results from the preceding sections, with two surveys that each *did* share one of these characteristics: the second Cambridge pulsar survey and the ATA "Fly's Eye" experiment.

The second Cambridge survey at 81.5 MHz (see Shrauner et al., 1998) is a relatively recent pulsar survey at low radio frequencies. The fact that it scanned the same northern sky as LPPS makes a comparison especially interesting. Of the sample of 20 pulsars detected in that survey, the blind periodicity search of LPPS data did not detect 4 pulsars, B0809+74, B0943+10, B1133+16 and B1642−03. The observation that contained B0809+74 was not fully processed because of problems with the data. An earlier, partial, processing of that data did yield the single pulse detection quoted in table 3.1. The observations that could have resulted in the detection of B0943+10 and B1133+16 were corrupted and pulsar B1642−03 fell outside of the area of sky surveyed by LPPS. The fact that LPPS detected a larger number of pulsars is perhaps unsurprising as LOFAR is a more sensitive instrument than the one used for the

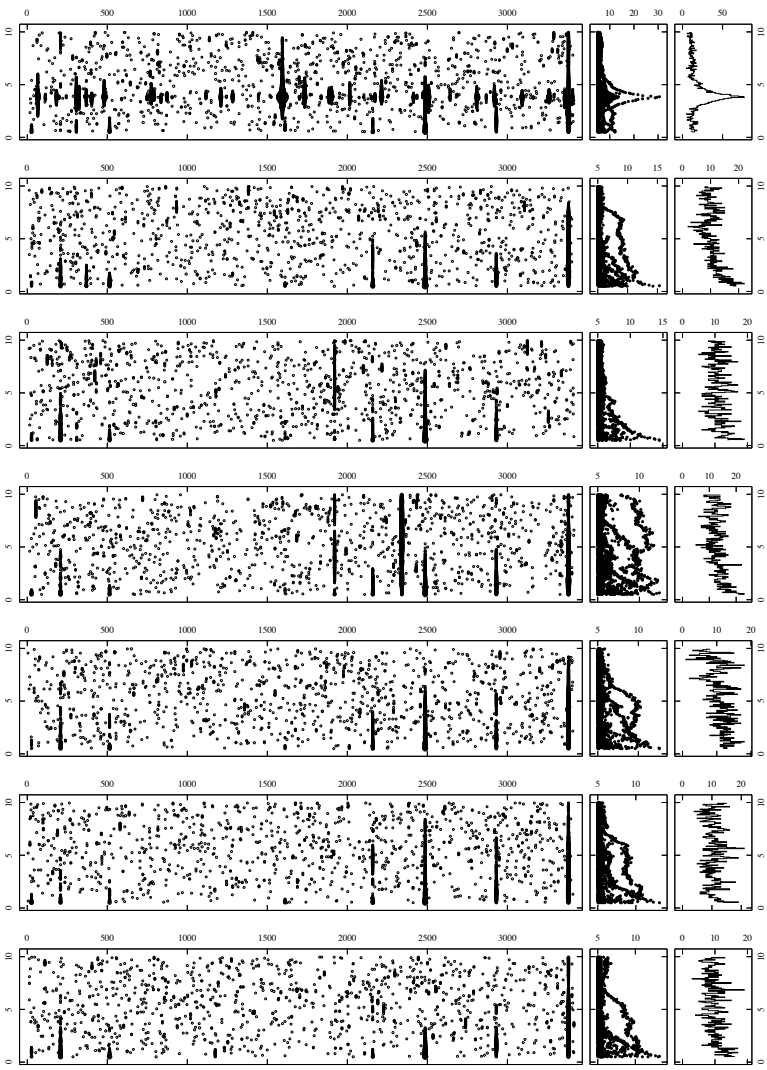

Figure 3.17: The single-pulse detections in observation L2010_21756, plotted between DMs of 0.5 cm^{-3} pc and 10 cm^{-3} pc. The top panel of the plot shows J0242+6256 clearly detected whilst the other beams show no detection, only some RFI.

second Cambridge pulsar survey, and the higher sky temperature for the Cambridge survey is also higher. Furthermore it is possible that some pulsars were detected by LOFAR because they were intrinsically brighter in the LPPS band, and turn over below it.
A unique feature of LPPS is its large FoV, and the almost 1-hr integration time. It shares those features with the "Fly's Eye" experiment that was carried out with the Allen Telescope Array (ATA, Welch et al., 2009) at a frequency of 1.4 GHz. There, 30 individual 6-m ATA dishes were pointed side-by-side to form an extended, 150 deg^2 strip on the sky at a constant declination. Celestial sources then drifted through that strip in about 6 hours. This experiment did not involve pulsar periodicity searches, but it performed single-pulse searches making it an L-Band equivalent of the LPPS single-pulse searches. Down to a signal-to-noise ratio of 8 no single pulse were detected from astronomical sources other than the pulsar B0329+54 (Siemion et al., 2012).

3.4.8 MODELING OF THE UNDERLYING PULSAR POPULATION

THE results presented above mean that LPPS was, on completion, the deepest large-area survey in the 100 MHz regime. The several dozen blind detections, of albeit known, pulsars constitutes a low-frequency sample that is now of adequate size to serve as statistical input for a pulsar population model.
Several approaches to population synthesis modeling exist. These all share two main features: they model both the underlying neutron star population, and the radio telescope's response. The models of the neutron star population can be derived in "snapshot" fashion, where the current pulsar population is directly modeled (e.g. Lorimer et al., 2006), or can start with an initial population whose spin-down, kinematics and luminosity are evolved over time and space throughout the last Gyr of our Galaxy (e.g. Bhattacharya et al., 1992; Faucher-Giguère & Kaspi, 2006). The subsequent modeling of the various radio telescopes' response is essential for determining which surveys could have detected which simulated pulsars. Survey sensitivity depends strongly on properties of the pulsar emission that are each linked to specific parts of the pulsar population, e.g.: moderate time sampling renders a survey insensitive to millisecond pulsars; wide channels prevent detection of high-DM sources; low frequency surveys will not find highly scattered sources. With these survey descriptions in place, the parameters of the input population are varied until a best-fit solution is found for the modeled and real survey results.
In modeling LPPS we used the dynamic, evolving model approach developed in Hartman et al. (1997). We populated the modeled Galaxy with a population of pulsars that van Leeuwen & Stappers (2010) found to best reproduce the survey results of 6

large surveys. We implemented a survey model of LPPS that takes into account the total footprint on the sky, including overlapping regions (Fig. 3.3); the distribution of usable integration times (Section 3.3.4); the sensitivity variation between pointings using different sets of stations; and the gain determined in Section 3.4.4. Based on the cumulative signal-to-noise values determined for our detected sample (Table 3.1), any simulated pulsar producing a SNR over 15 was labeled detected.
In our simulation, 2.7 million pulsars formed throughout the Galaxy. Of these, 50,000 were above the death line at the present day and beamed toward Earth; 9,000 are in our survey FoV. For 1,200 of these, the scatter and dispersion broadening exceeds their rotational period, making them undetectable. Of the remaining 8,000 pulsars, 80 are bright enough to be detected in LPPS. Running the simulation over the error range on the derived gain of 0.60 ± 0.13 K/Jy produces a LPPS detected sample containing 80 ± 20 pulsars. That is in reasonable agreement with the actually detected number of 54; while some of the difference between these numbers could be in either the modeled survey (e.g., remaining incomplete understanding of the incoherent-addition of this commissioning era data) or the modeled population (e.g., the low-frequency spectrum turn-over behaving differently than simulated). Overall, these simulations confirm that our best pulsar population models can accurately predict low-frequency surveys (van Leeuwen & Stappers, 2010).

3.5 DISCUSSION

THE detection of 54 pulsars in the blind search of the LPPS data has demonstrated that LOFAR is a capable pulsar search instrument. In particular the independent discovery of PSR J2317+68 highlights the fact that LOFAR is competitive with the state-of-the-art in pulsar searches of the northern celestial hemisphere conducted with the GBT. LOFAR also detected all pulsars in the sample of the second Cambridge pulsar survey (Shrauner et al., 1998), except for those few pulsars whose position was not observed or that were in corrupted data. The further detection of 9 pulsars by folding on their known ephemerides means that our processing can still be improved to better extract pulsars from spurious, RFI-related candidates. As LOFAR now routinely produces better-calibrated, more sensitive data, the prospects for achieving a significantly deeper all-sky survey using the same incoherent beam-forming technique as LPPS is very good.
In the single pulse-search, 20 pulsars were detected. This means that we were able to detect about one third of our periodicity search detections in single-pulse searches of the same data. This is in line with predictions from Stappers et al. (2011). In particular,

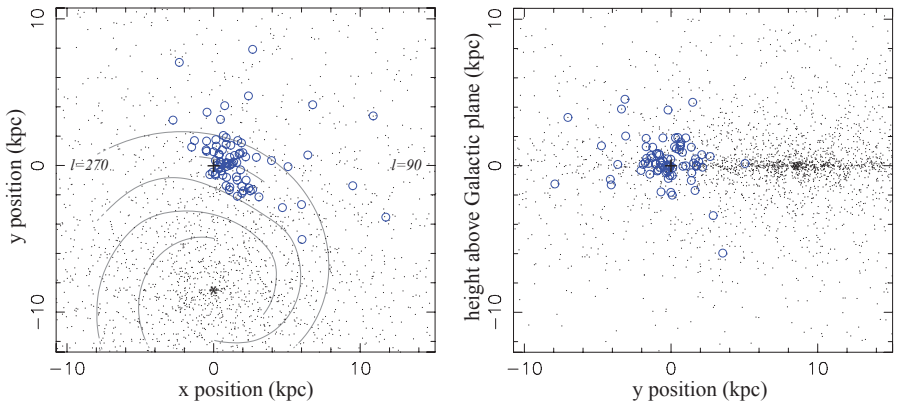

Figure 3.18: The modeled pulsars in our Galaxy. Pulsars that are still emitting at the current time, and are beamed toward us, are marked with dots (only 10% of these shown). Pulsars that are detected in LPPS are marked with blue open circles. The Earth is marked with a '+', the Galactic center with a '*'. On the left a projection onto the plane of the Galaxy is plotted, including spiral arms, with the Galactic centre at y=-8.5 kpc from the Earth. The right hand panel shows the projection of the detections onto the vertical plane through the Galactic centre and the Earth.

the nearby, low-luminosity pulsar J0242+6256 stood out as having unexpectedly bright pulses in the LPPS band. With the long dwell times that can be afforded by the huge FoV of LOFAR's incoherent beam-forming mode, the prospects for discovering other intermittent but occasionally bright sources like PSR J0242+6256 are also very good.

Since LPPS covered a large part of the sky with long integrations it is more sensitive to infrequent events than typical pulsar surveys with shorter dwell times. We attempted a search for bright, dispersed radio bursts but did not find any. This allowed us to derive an upper limit to the occurrence of bright dispersed radio bursts in the absence of strong scattering. The limit we found, 1.5×10^2 bursts per full sky per day brighter than 107 Jy is in line with limits found by other surveys. In ongoing LOFAR transient searches, we are continuing to improve on this limit and better constrain the spectra and scattering properties of such bursts. These searches will either soon detect such signals or show that the higher-frequency ($\sim$ 1.4 GHz) window is ideal for their detection.

During the processing the LPPS survey it was quite apparent that a sizable fraction of

the data was badly affected by RFI or start-up hardware and software problems with the telescope. Had this not been the case, LPPS would have been more sensitive by a factor of roughly two to three. Indeed, the second LOFAR pulsar commissioning survey, LOFAR Tied-Array Survey (LOTAS, see Chapter 4), was much less affected by bad data than LPPS. At the time of this writing, LOFAR is no longer in its commissioning phase and is working through its Cycle 0 science observations. Among the projects currently being observed is the LOFAR Tied Array All-sky Survey (LOTAAS). This survey uses tied-array (coherent) beam-forming, but also contains an LPPS-like component where incoherent beams are simultaneously created using the LOFAR Superterp. While fewer instantaneous beams are used — only 3 for LOTAAS — this incoherent part of this survey will be at least two times more sensitive than LPPS because more bandwidth is used per beam (32 MHz per beam versus only 6.8 MHz for LPPS), the stations are now well calibrated and hence performing closer to their theoretical sensitivity, and each part of the sky will be observed 3 times to look for intermittent or transient sources.

3.6 CONCLUSIONS AND FUTURE WORK

DURING LOFAR's commissioning period, we have performed a pulsar survey: LPPS, the LOFAR Pilot Pulsar Survey. Survey processing yielded the re-detection of 54 pulsars in the periodicity search, of which 18 were also detected in single pulse searches, 2 pulsars were detected only through their single-pulse emission and a further 9 pulsars were retrieved from the data by folding on known ephemerides.
LOFAR is the premier low-frequency telescope in a new generation of sophisticated radio observatories leading to the construction of the SKA. Since LOFAR, much like SKA in the future, is a software telescope with flexible digital beam-forming capabilities it acts as a proving ground for new surveying strategies. It is expected that the first phase of the SKA will included a sparse low-frequency aperture array, containing up to a quarter million antenna elements that are beam-formed into stations in a LOFAR-like way. The core of this low-frequency array will be easily 16 times more sensitive than the LOFAR core and will be an unprecedented pulsar survey and timing machine.